TECHNISCHE MECHANIK
an open access journal

journal homepage: www.ovgu.de/techmech

Tech. Mech., Vol. 40, Is. 1, (2020), 97–107

Received: 30.07.2019
Accepted: 05.12.2019
Available online: 20.02.2020

Computation of Cauchy heterogeneous stress field in a cruciform specimen subjected to equibiaxial tensile within parameter identification of isotropic hyperelastic materials

Kamel Yaya[1]*, Hocine Bechir[1], and Safia Bouzidi[1]

[1]Laboratoire de Mécanique, Matériaux & Énergétique (L2ME), Faculté de Technologie, Université de Bejaia, 06000, Bejaia, Algeria

Abstract: Heterogeneous stress and strain fields have been investigated by Finite Element Method (FEM) in a cruciform specimen holed at the center and subjected to equibiaxial tensile. The stress field is zero at the boundary of the hole; it is a useful boundary condition to compute local stress field. Also, the heterogeneity proves out to be an advantage in order to increase the variety of deformation states. So, a digital image correlation (DIC) system could provide the local deformations, and the corresponding stress field was optimized and adapted to the specimen geometry. Indeed, on the basis of FE results, the heterogeneous Cauchy stress field has been computed analytically in a sub-core region of the sample. As a result, the local strain and stress fields may be related; so that, the material parameters of isotropic and incompressible rubber-like materials could be identified from experimental data arising from a single heterogeneous test. Besides, the key ideas have been highlighted in order to solve the inverse problem related to the identification procedure.

Keywords: Hyperelasticity, Multiaxial testing, Heterogeneous fields, Finite element method, Analytic, Parameter identification

1 Introduction

Modeling the behavior of elastomeric materials is commonly carried out within the framework of hyperelasticity, cf. Ogden (1997); Holzapfel (2000). Nevertheless, the parameter identification is still difficult task, cf. Hartmann and Gilbert (2018). It should be noticed that, the numerical values of these parameters are input-data of the FE-codes. Due to the multi-axial behavior of elastomeric materials, accurate mechanical test data is crucial for both obtaining the model form and model parameter calibration. Standard tests related with this purpose require sample geometries that can lead to homogeneous deformations (uni-axial tensile, pure shear and equi-bi-axial tensile), cf. Galliot and Luchsinger (2011); Sasso et al. (2008). In practice, the constitutive parameters that are identified with those three types test performed separately are generally different, cf. Guo and Sluys (2006).

To bypass the problem, the material parameters could be identified from experimental data of the biaxial tensile test in order to ensure predictive ability of a hyperelastic model, cf. Seibert et al. (2014). We emphasize that, the biaxial testing was performed on cruciform specimens. So, the heterogeneous deformation states of equibiaxial tensile test and an inverse method (so-called, the virtual fields method) have been used, cf. Promma et al. (2009), in order to compute the Mooney-Rivlin model constants, cf. Mooney (1940). Nevertheless, the Mooney-Rivlin model does not suitable to reproduce the multi-axial behavior of elastomeric materials; so that, more than two parameters are required in the range of large strains. We notice that an optimal shape of a cruciform specimen depends on its geometry and specific constraints that are imposed by the cutting or molding. The computation of deformation and stress states in core region of cruciform specimen is a subject of debate, cf. Seibert et al. (2014); Hu et al. (2014); Hartmann et al. (2018) (and the literature cited therein). The strains distribution seems to be uniform; nevertheless, the corresponding stress distribution does not. Thereby, the biaxial tensile test seems to give rise to heterogeneous stress and strain fields even near core region of a cruciform sample. Therefore, we cannot establish a relationship between the local stresses in central region and applied forces on the arms of a cruciform sample, even by assuming that the strains are homogeneous in a small core area of the test specimen, and the corresponding stress distribution is homogeneous too (for homogeneous, elastic materials). Nowadays, digital image correlation (DIC) is a powerful experimental technique to determine displacement and deformation fields in solids, cf. Hild and Roux (2006); it provides full field displacement and deformation values. Consequently, it is straightforward to determine the in-plane components of the deformation gradient; however, its corresponding stress state is undetermined. A simplified method has been proposed by Chevalier et al. (2001) to evaluate a quasi-uniform Cauchy stress, so-called σ_B, in core region of a cruciform specimen. Recently, both experimental study and finite element analysis have shown that a homogeneous stress distribution cannot be obtained in near center of a cruciform sample. So the computation of stresses represents a critical issue for biaxial tensile tests. Indeed, no method to date addresses the relationship between the applied forces and the stress state in core region of a cruciform specimen, cf. Hartmann et al. (2018). As a result, errors made in the computation of stress tensor components will propagate into the parameter identification, ultimately limiting our ability to accurately simulate the hyperelastic behavior of elastomeric materials.

This work concerns with an original computation method of Cauchy stresses around a small circular hole in a cruciform sample subjected to equibiaxial tensile. The hole (of radius a) is located in the center; that is leading to increase the heterogeneity of strain field, which is assumed to be provided by a DIC-system. As a result, heterogeneity turns out to be an advantage to analyze both the

* E-mail address: kamel.yaya@univ-bejaia.dz
doi: 10.24352/UB.OVGU-2020-018

stresses state and deformations distribution around the hole. We show that the proposed stress field can be used for the parameter identification of isotropic hyperelastic solids. To be clear, we consider a core area of radius ρ around the hole that is located between the extremity of such hole to the intersection of the arc whose center is the intersection of the arms and that is tangent to these arms. In the core region, we will compute the Cauchy stresses numerically by FE: $\sigma_{rr}(\xi,\theta)$, $\sigma_{r\theta}(\xi,\theta)$ and $\sigma_{\theta\theta}(\xi,\theta)$ by using the generalized Gent model, cf. Gent (1996). Based on these numerical results, we show that, it is possible to formulate analytically a Cauchy stress field in a core region around the hole. The stress field is depending on the spatial variables $\xi = r/\rho$ and θ, distribution of nominal traction along border of arms, i.e. $\sigma_{\mathbf{U}}$ and geometrical parameter, i.e. a/ρ. As a consequence, the parameter identification is reduced to solving an inverse problem by combining both the data provided by DIC-system and of proposed stresses field. Also, we could use the data arising from this heterogeneous test in order to validate known hyperelastic constitutive equations.

2 Material modeling

In continuum mechanics, the mechanical properties of elastomeric materials are described in terms of strain-energy density function Ψ, cf. Ogden (1997); Holzapfel (2000). For isotropic elastic material, depends on the strain principal invariants

$$\mathrm{I}_1 = \mathrm{tr}(\boldsymbol{B}), \mathrm{I}_2 = 1/2\left[(\mathrm{tr}(\boldsymbol{B}))^2 - \mathrm{tr}\left(\boldsymbol{B}^2\right)\right], \mathrm{I}_3 = \det(\boldsymbol{B}) \tag{1}$$

where $\boldsymbol{B} = \boldsymbol{F}\boldsymbol{F}^T$ is the left Cauchy-Green tensor and $\boldsymbol{F}$ is the gradient of the deformation.
Rubber-like materials are often assumed to be incompressible provided that the hydrostatic stress does not become too large and so the admissible deformations must be isochoric, i.e. $\det(\boldsymbol{F}) = 1$ so that $\mathrm{I}_3 = 1$. Cauchy stress of an incompressible isotropic elastic material can be determined as follows:

$$\sigma = -p\boldsymbol{I} + 2\Psi_{,1}\boldsymbol{B} - 2\Psi_{,2}\boldsymbol{B}^{-1} \tag{2}$$

where p is the Lagrange multiplier, $\boldsymbol{I}$ is the identity tensor and $\Psi_{,i} = (\partial\Psi/\partial \mathrm{I}_i)_{i=1,2}$ are the partial derivatives of the strain-energy density function.
We consider the phenomenological model of Gent, cf. Gent (1996) which is able to represent limiting chain extensibility of the molecular chains; its strain-energy density is

$$\Psi = \frac{\mu_0}{2}\left[-\alpha J_m \ln\left(1 - \frac{\mathrm{I}_1 - 3}{J_m}\right) + (1-\alpha)(\mathrm{I}_2 - 3)\right] \tag{3}$$

where μ_0 is the shear modulus for infinitesimal deformations, $\alpha \in]0, 1]$ is a dimensionless constant and J_m is the limiting value of $\mathrm{I}_1 - 3$, taking into account limiting polymeric chain extensibility. On taking the limit $J_m \to \infty$ in Eq. (3), we recover the well-known Mooney-Rivlin model, cf. Mooney (1940). For further discussion of Eq. (3) and related constitutive models, (see Horgan and Saccomandi (1999, 2001)) where the solutions to the torsion, axial shear and circular shear problems have been obtained.

2.1 Finite element simulations

A finite element calculation is performed by assuming both plane stress state and a nearly incompressibility approach. Thus, a mixed formulation pressure-displacement was used in order to avoid element locking. For that purpose, the strain-energy density function is decomposed into an isochoric and volumetric parts. To this end, we declare the model of Eq. (3) as slight compressible by replacing the principal invariants I_1 and I_2 by equivalent invariant ones, cf. Simo and Hughes (2006). Consequently, the strain-energy density function has been decomposed as the sum of the two energies related to distortional and dilatational deformations, so that Eq. (3) becomes

$$\Psi = \tilde{\Psi}\left(\bar{\mathrm{I}}_1, \bar{\mathrm{I}}_2\right) + \hat{\Psi}(\mathrm{J}) \tag{4}$$

where $\bar{\mathrm{I}}_1 = \mathrm{I}_1 \big/ \mathrm{I}_3^{1/3}$ and $\bar{\mathrm{I}}_2 = \mathrm{I}_2 \big/ \mathrm{I}_3^{2/3}$.
We point out that, $\tilde{\Psi}\left(\bar{\mathrm{I}}_1, \bar{\mathrm{I}}_2\right) = (\mu_0/2)\left\{\left[-\alpha J_m \ln\left(1 - \left(\left(\bar{\mathrm{I}}_1 - 3\right)/J_m\right)\right)\right] + (1-\alpha)\left(\bar{\mathrm{I}}_2 - 3\right)\right\}$ and $\hat{\Psi}(\mathrm{J}) = (\kappa_0/2)(\mathrm{J}-1)^2$, where κ_0 is the bulk modulus. The strain-energy density function (Eq. (4)) was implemented in a FE code. First, we used the material constants of Mooney-Rivlin model, cf. Mooney (1940), i.e. $c_{10} = \alpha\mu_0/2$ and $c_{01} = (1-\alpha)\mu_0/2$ of a Silicone rubber that are given in Seibert et al. (2014), and by varying the material constant, i.e. J_m (see, Tab. A.1). Also, these authors have designed and optimized cruciform shape specimen in order to obtain quasi-homogeneous strain state in the core region. Consequently, the numerical simulations were performed on a cruciform specimen defined by the circle of radius $R = 18.75\,mm$, length $L_0 = 25\,mm$ and hole of radius $a = 0.01\rho$ ($\rho = 16.66\,mm$); the thickness of the sample is assumed uniform ($e_0 = 2\,mm$). For symmetry reasons, only one quarter of the specimen is taken into account. The geometry and the boundary value problem including boundary and symmetry conditions are shown in Fig. 1. The displacements $U_1 = U_2 = U$ are prescribed in the extremities of the arms in order to ensure equibiaxial loading conditions. Boundary conditions were applied on the nodes that were in perfect contact (no slip) with the clamps. The deformed specimen is depicted in Figs. 2 along with initial shape to illustrate that large strains exist in the core region. The components of the Green-Lagrange strain tensor, i.e. $\boldsymbol{E}_{11}$, $\boldsymbol{E}_{12}$ and $\boldsymbol{E}_{22}$ are obtained from finite element results, are shown in Figs. 3 versus dimensionless radius ξ for different values of θ. We notice that, the large strains are located

near the hole; and the strain state is highly heterogeneous in the core region of radius ρ. The component $\boldsymbol{E}_{11}$ has a minimum and increases gradually in the ξ-direction from the side of the hole. While the component $\boldsymbol{E}_{22}$ decreases and showing an opposite behavior with respect to the corresponding $\boldsymbol{E}_{11}$. Due to the large deformability of elastomeric materials, the specimen may rotate causing some shearing, i.e. $\boldsymbol{E}_{12}$, that reach a maximum near the hole. The shear strain $\boldsymbol{E}_{12}$ depends on the radius ρ (or R), near

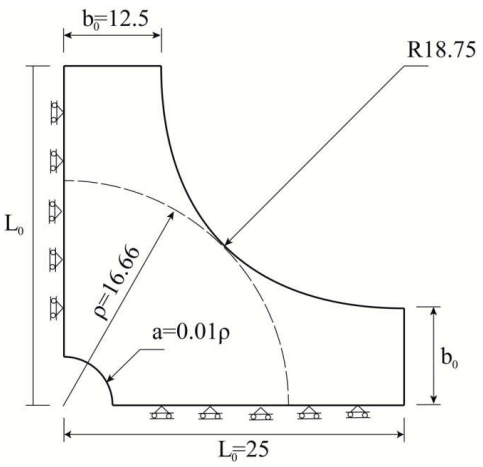

Fig. 1: One quarter of the cruciform specimen, a small hole is located in the center of the sample with applied boundary conditions

core region of the sample, if $R \ll L_0$ then $\boldsymbol{E}_{12}$ tends to zero, so that, planar-biaxial stretching of the cruciform sample may be considered as a "perfect" equibiaxial tension. Consequently, the effects of free and clampedF edges influence the strain and stress fields in the sample. We notice that, the shear deformations are zero on the symmetry axes of the sample, i.e. $\theta = 0$ and $\theta = \pi/2$. Ideally, the specimen subjected to equibiaxial stretching (without hole and $R \ll L_0$) should not develop local rigid-body-rotation. Let us analyze the stress state in the core area of radius ρ around the hole. The Cauchy stresses i.e. $\sigma_{11}(x, y)$, $\sigma_{12}(x, y)$, $\sigma_{22}(x, y)$ and the mean value of the nominal stress σ_U at the extremity of one arm are inferred from the FE-simulations. Thereafter, the Cauchy stresses are computed in polar coordinates as follows:

$$\begin{pmatrix} \sigma_{rr}(r,\theta) & \sigma_{r\theta}(r,\theta) \\ \sigma_{r\theta}(r,\theta) & \sigma_{\theta\theta}(r,\theta) \end{pmatrix} = \begin{pmatrix} \cos\theta & \sin\theta \\ -\sin\theta & \cos\theta \end{pmatrix} \begin{pmatrix} \sigma_{11}(x,y) & \sigma_{12}(x,y) \\ \sigma_{12}(x,y) & \sigma_{22}(x,y) \end{pmatrix} \begin{pmatrix} \cos\theta & -\sin\theta \\ \sin\theta & \cos\theta \end{pmatrix} \tag{5}$$

where σ_{rr}, $\sigma_{r\theta}$ and $\sigma_{\theta\theta}$ are respectively, radial, shear and hoop Cauchy stresses, $x = r\cos\theta$, $y = r\sin\theta$ and $\tan\theta = y/x$. The results are shown in Figs. 4 for the radial stress, shear stress and hoop stress versus dimensionless radius ξ for different values of θ. Accordingly, no shear is observed on the symmetry axes of the sample corresponding to the directions of $\theta = 0$, $\pi/4$ and $\pi/2$. Radial stress reaches its maximum on the symmetry axes of the sample ($\theta = 0$ and $\theta = \pi/2$); also the free edge condition leads to $\sigma_{rr}(\xi = 1,\ \theta = \pi/4) = 0$. Hoop stress reaches maximum on the edge of the hole and tending to zero far from the hole. We point out that, the presence of the hole requires satisfying the following boundary conditions:

$$\sigma_{rr}(\xi_a = a/\rho, \theta) = \sigma_{r\theta}(\xi_a = a/\rho, \theta) = 0 \tag{6}$$

We notice that, the presence of the hole requires satisfying the following boundary conditions:

$$\sigma_{rr}(\xi_a = a/\rho, \theta) = \sigma_{r\theta}(\xi_a = a/\rho, \theta) = 0 \tag{7}$$

In Fig. 5, we plot the nominal stress i.e. $\sigma_U = \langle force\rangle / e_0 b_0$ versus a prescribed displacement U and by varying the material constant J_m; $\langle Force\rangle$ is the mean applied force on the nodes of an arm. On taking the limit of $J_m = 500$ in Eq. (3), the well-known Mooney-Rivlin model, cf. Mooney (1940) is recovered.

2.2 Construction of an approximation of Cauchy stress field

The computation of Cauchy stress field around a hole has been well established in the framework of linear elasticity theory, cf. Timoshenko (1951). However, finding stress field in the framework of isotropic hyperelasticity remains scarce in the literature. In this paper, we propose an analytical approximation of Cauchy stress field in the core sub-region of the dimensionless radius ξ ($0.01 \leq \xi = r/\rho \leq 0.5$) around the hole. First, consider the equilibrium equations in the deformed configuration

$$\frac{\partial \sigma_{rr}}{\partial r} + \frac{1}{r}\frac{\partial \sigma_{r\theta}}{\partial \theta} + \frac{1}{r}(\sigma_{rr} - \sigma_{\theta\theta}) = 0 \tag{8}$$

$$\frac{\partial \sigma_{r\theta}}{\partial r} + \frac{1}{r}\frac{\partial \sigma_{\theta\theta}}{\partial \theta} + \frac{2}{r}\sigma_{r\theta} = 0 \tag{9}$$

We may re-arrange the Eqs. (8) and (9) to get:

$$\sigma_{\theta\theta} = \frac{\partial \sigma_{r\theta}}{\partial \theta} + r\frac{\partial \sigma_{rr}}{\partial r} + \sigma_{rr} \tag{10}$$

$$\frac{\partial}{\partial \theta}\left(r\frac{\partial \sigma_{rr}}{\partial r} + \sigma_{rr}\right) = -\left(2\sigma_{r\theta} + r\frac{\partial \sigma_{r\theta}}{\partial r} + \frac{\partial^2 \sigma_{r\theta}}{\partial \theta^2}\right) \tag{11}$$

Accordingly, the radial stress and hoop stress are inferred from the shear stress. By using the previous FE-results, we may express the shear stress as follows:

$$\sigma_{r\theta}(\xi, \theta) = -\sigma_U h(\xi) \sin 4\theta \quad \text{for} \quad 0.01 \leq \xi \leq 0.5 \tag{12}$$

where σ_U and $h(\xi)$ are respectively, the nominal stress tensile along border of arms and an unknown function to be determined. We emphasize that the function $h(\xi)$ is arising from the results of finite element simulations. It was shown that this function does not depend on both Jm, and θ for $(0.01 \leq \xi = r/\rho \leq 0.5)$. Therefore, we may assume that the function $h(\xi)$ does not depend on the strain energy function.
The function $h(\xi)$ can be evaluated as follows:

$$h(\xi) = -\frac{\sigma_{r\theta}}{\sigma_U \sin 4\theta} \quad \text{for} \quad \theta \neq 0,\ \pi/4 \text{ and } \pi/2 \tag{13}$$

where $\sigma_{r\theta}$ is arisen from the FE-simulations.
$h(\xi)$ can be approximated with respecting the boundary conditions as follows:

$$h(\xi) = \beta\lambda(\xi - \xi_a)^2 \tag{14}$$

where $\lambda = 1 + \frac{U}{L_0}$ is the macroscopic stretch ratio and β is adjustable numerical constant.
The graphs of the function $h(\xi)$ versus ξ for $\theta \neq 0$, $\pi/4$ and $\pi/2$ and $\beta \approx 0.447$ are shown in Fig. 6. Noticing that, the graphs of $\frac{h(\xi)}{\lambda}$ are not depending on magnitude of displacement U, θ, and material constant, J_m. As a consequence, the variable separation of Eq. (13) seems to be reliable.
By substituting the Eqs. (12) and (14) into Eq. (11), we obtain the following differential equation:

$$\xi\frac{\partial \sigma_{rr}}{\partial \xi} + \sigma_{rr} = \frac{\sigma_U}{4}(14h(\xi) - \xi h'(\xi))\cos 4\theta + f(\xi) \tag{15}$$

Where $f(\xi)$ is a function to be determined and $\sigma_{rr}(\xi = \xi_a, \theta) = 0$.
The solution of Eq. (15) is

$$\sigma_{rr}(\xi, \theta) = \left(\frac{\sigma_U}{4}\beta\lambda\right)\left(4\xi^2 + 14\xi_a^2 - 13\xi_a\xi - 5\xi_a^3\xi^{-1}\right)\cos 4\theta + F(\xi) \tag{16}$$

where $F(\xi)$ is inferred from the results of FE-simulations of radial Cauchy stress, i.e. $\sigma_{rr}(\xi, \theta)$ (see, **Appendix A**).

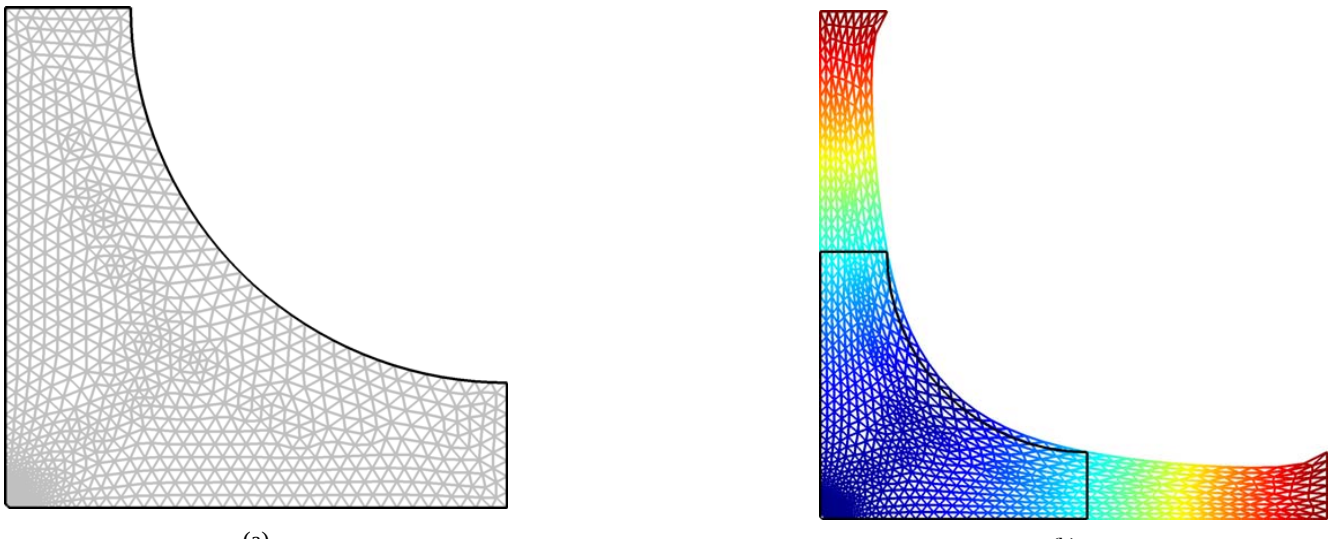

(a) (b)

Fig. 2: (a) The undeformed specimen in the reference configuration and meshes of plane stress problem; (b) The deformed specimen in the current configuration for $U_1 = U_2 = U = 25\ mm$

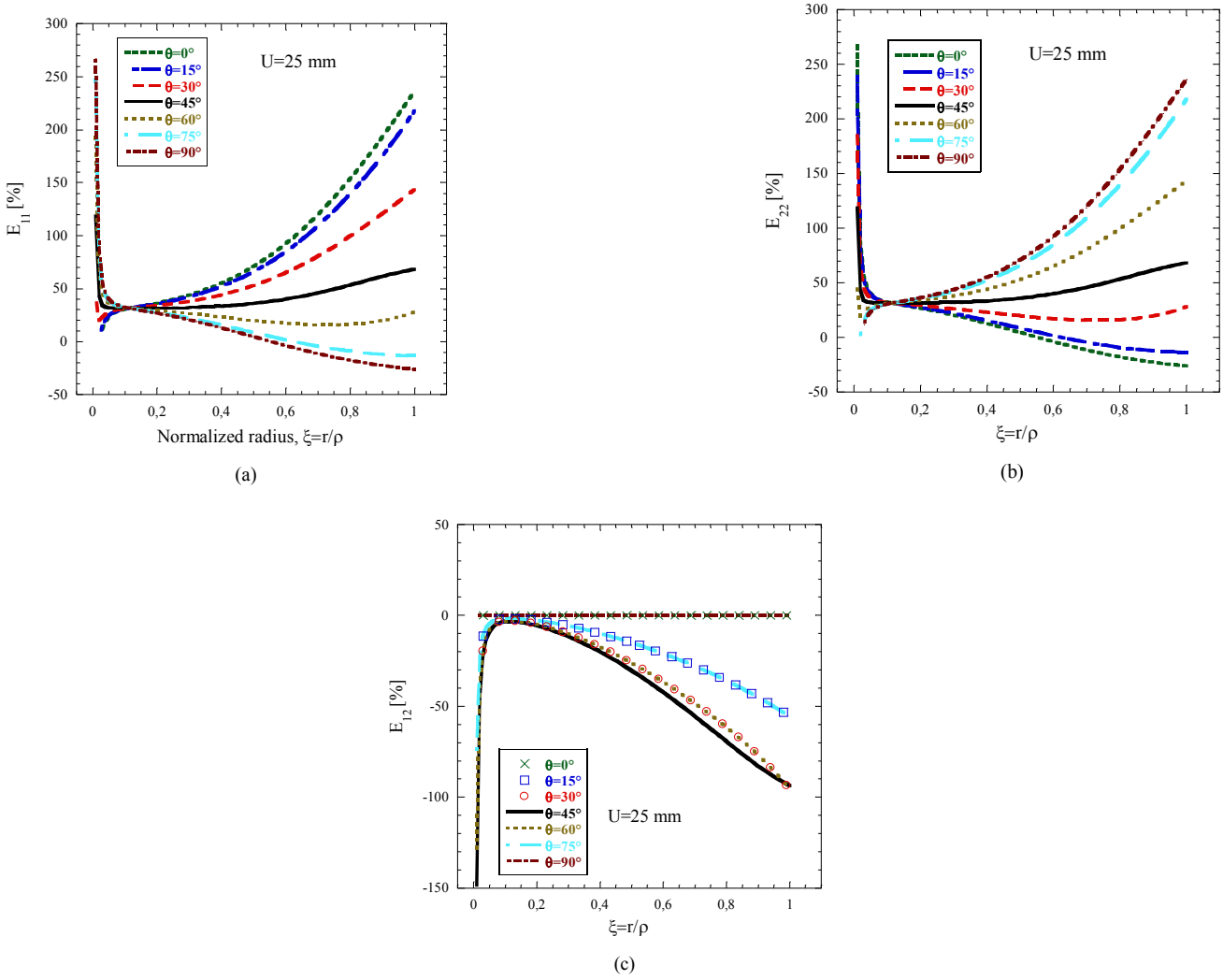

Fig. 3: Plots of the Green-Lagrange strain tensor component $\boldsymbol{E}_{ij}$ versus normalized radius ξ for $U_1 = U_2 = U = 25\ mm$; (a) Component $\boldsymbol{E}_{11}$ versus normalized radius ξ; (b) Component $\boldsymbol{E}_{22}$ versus normalized radius ξ; (c) Component $\boldsymbol{E}_{12}$ versus normalized radius ξ

We get the hoop stress by substituting Eqs. (16) and (12) into Eq. (10)

$$\sigma_{\theta\theta}\left(\xi,\theta\right) = \left(\frac{\sigma_U}{4}\beta\lambda\right)\left(-4\xi^2 - 2\xi_a^2 + 6\xi_a\xi\right)\cos 4\theta + F\left(\xi\right) + \xi\, F'\left(\xi\right) \tag{17}$$

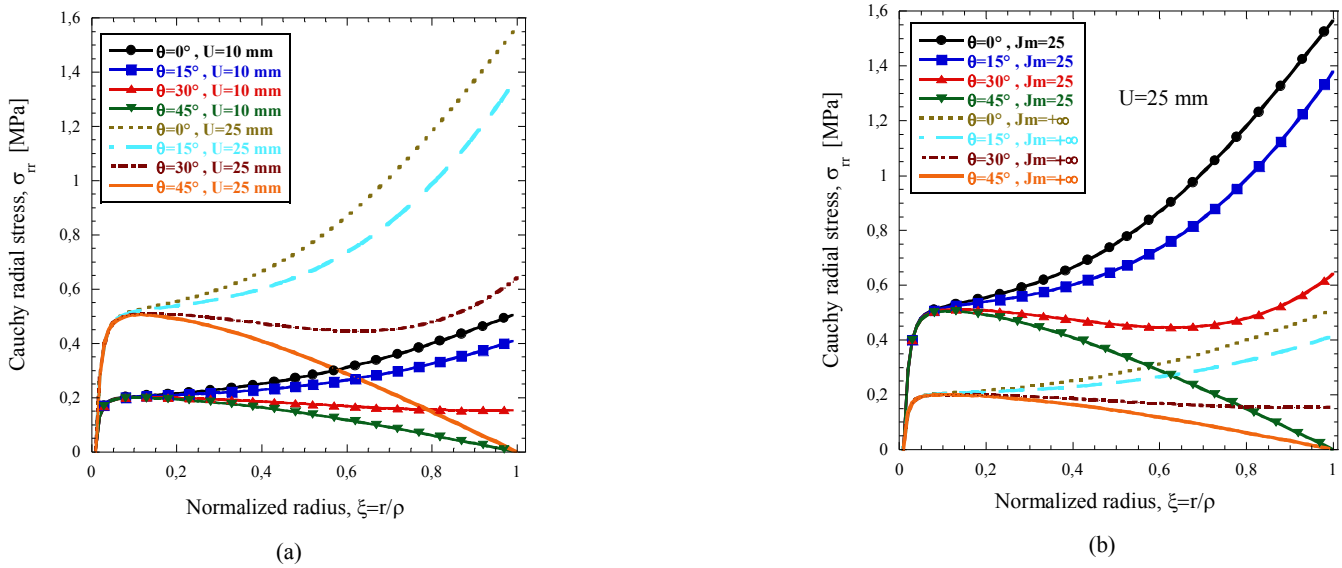

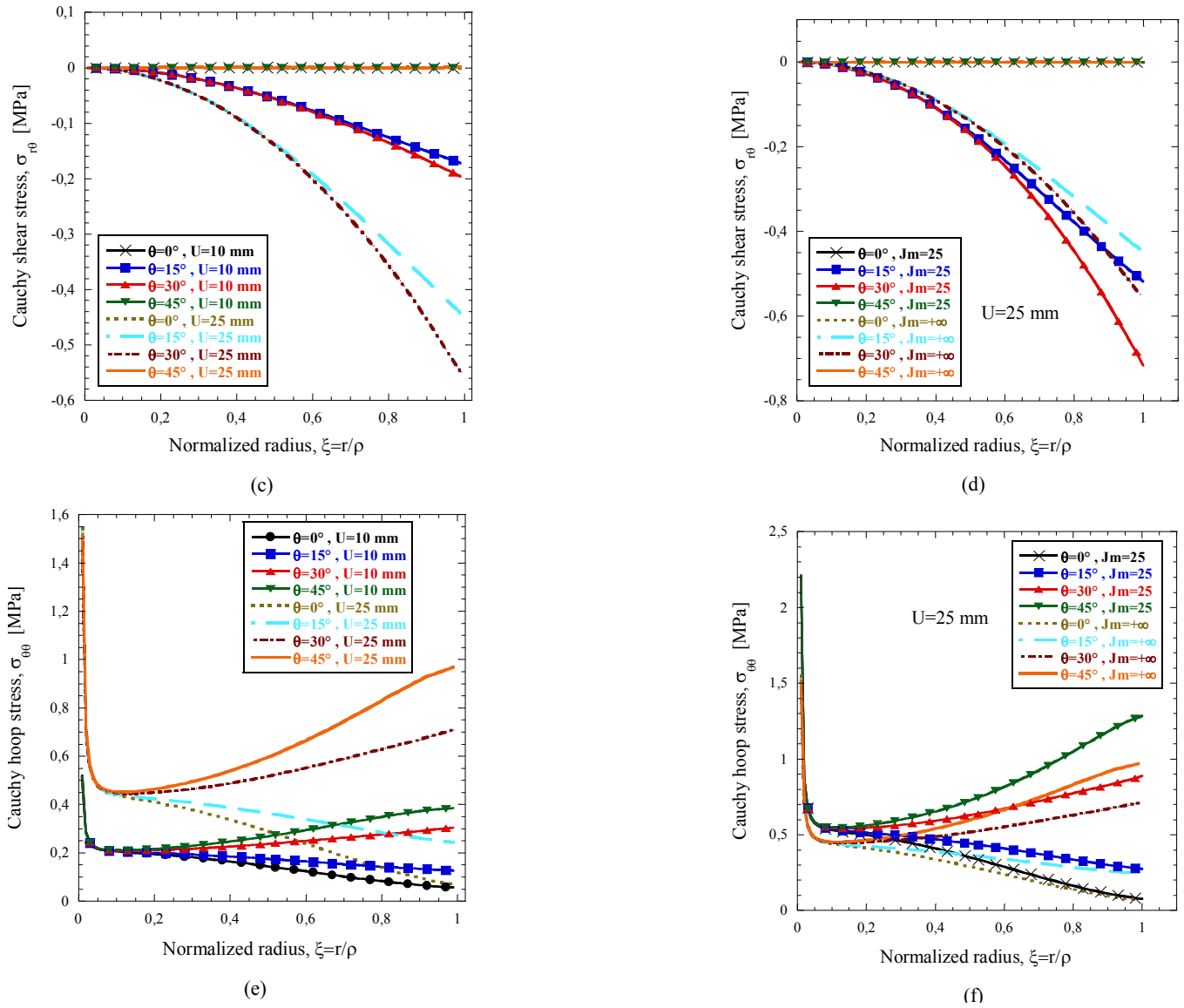

Fig. 4: (a) Cauchy radial stress, $\sigma_{rr}(\xi,\theta)$ versus normalized radius ξ for different values of θ and U; (b) Cauchy radial stress, $\sigma_{rr}(\xi,\theta)$ versus normalized radius ξ for different values of θ and J_m; (c) Cauchy shear stress, $\sigma_{r\theta}(\xi,\theta)$ versus normalized radius ξ for different values of θ and U; (d) Cauchy shear stress, $\sigma_{r\theta}(\xi,\theta)$ versus normalized radius ξ for different values of θ and J_m; (e) Cauchy hoop stress, $\sigma_{\theta\theta}(\xi,\theta)$ versus normalized radius ξ for different values of θ and U; (f) Cauchy hoop stress, $\sigma_{\theta\theta}(\xi,\theta)$ versus normalized radius ξ for different values of θ and J_m

The Cauchy stresses are explicitly given in **the Appendix A**. We notice that, the proposed stress field seems to be reliable to reproduce the FE-results in the core sub-region as shown in Figs. 7. This approximate stress field adapted to the test specimen geometry depends on prescribed displacement, i.e. U, resulting nominal stress, i.e. σ_U and geometrical ratio a/ρ. So, we may assume that, the Cauchy stress field does not depending on analytical form of strain-energy density function, since the stress state can be inferred from the geometrical variables alone and the applied force on the arms. Therefore, the data arising from this heterogeneous test can be exploited advantageously for the parameter identification. Real elastomeric materials typically exhibit time-dependent behavior due to viscous effects, implying that the strain and stress fields would not necessarily vary similarly. For instance, biaxial tensile test has been performed by Johlitz and Diebels, cf. Johlitz and Diebels (2011) in order to characterize effect of time on the behavior of a silicone rubber for which the viscoelasticity is nearly negligible. However, the analysis requires the mechanical properties of the material a priori. Thus not applicable approach if the "real" properties of the material have not yet to be determined. Besides, the proposed identification procedure could be extended to viscoelastic elastomers on the basis of a constitutive equation; so, we will solve a boundary value problem that can be challenging to achieve computationally.

3 New procedure of parameter identification

The material parameters of Mooney-Rivlin model can be estimated on basis of experimental data of the biaxial tensile, cf. Seibert et al. (2014); Promma et al. (2009). This heterogeneous single test has an advantage because three types of strain states coexist: uniaxial tensile, pure shear and equi-bi-axial tensile in different regions of the deformed sample. Consequently, we obtain weighted average values of model parameters; with comparison to the parameters that could be determined from the tests performing separately. We show that the partial derivatives of strain-energy densities can be determined without knowing their analytical

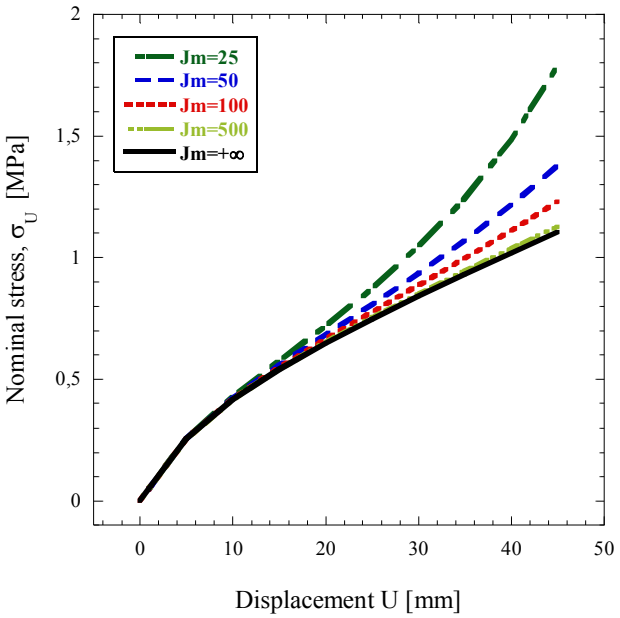

Fig. 5: Plots of nominal stress σ_U versus displacement U for different values of J_m

forms a priori. Moreover, the present approach can also be used for validation of hyperelastic models. We provide additional insights in order to explain the method of parameter identification. We assume that the deformation is relatively homogeneous around a material point in the framework of DIC measurements. As result, we may write the deformation gradient tensor of the planar biaxial test, cf. Zhang et al. (2015) as follows:

$$(F) = \begin{pmatrix} \frac{\partial x_1}{\partial X_1} & \frac{\partial x_1}{\partial X_2} & \frac{\partial x_1}{\partial X_3} \\ \frac{\partial x_2}{\partial X_1} & \frac{\partial x_2}{\partial X_2} & \frac{\partial x_2}{\partial X_3} \\ \frac{\partial x_3}{\partial X_1} & \frac{\partial x_3}{\partial X_2} & \frac{\partial x_3}{\partial X_3} \end{pmatrix} = \begin{pmatrix} \lambda_1 & \gamma_1 & 0 \\ \gamma_2 & \lambda_2 & 0 \\ 0 & 0 & \lambda_3 \end{pmatrix} \tag{18}$$

where X_k and x_k are coordinates for material particles in the reference and current configuration, respectively, λ_k and γ_k are the stretch ratios and amount of shears, respectively.

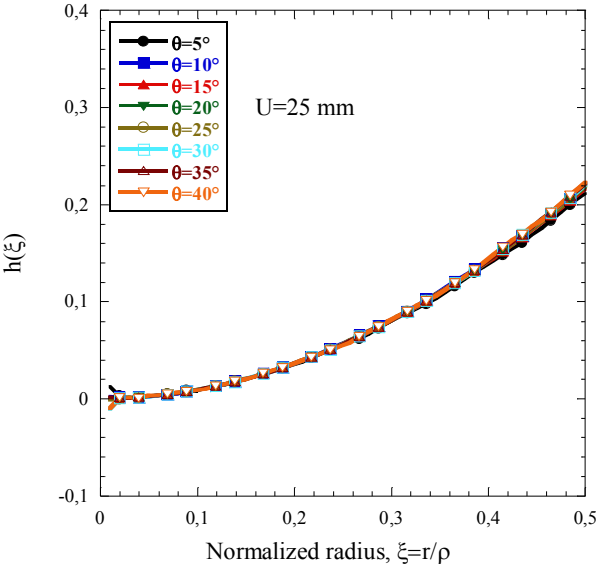

Fig. 6: Graphs of the function $h(\xi)$ versus normalized radius ξ

If we assume that the material is incompressible, i.e. $\mathrm{J} = \det(\boldsymbol{F}) = 1$, we may write

$$\mathrm{J} = \begin{vmatrix} \lambda_1 & \gamma_1 & 0 \\ \gamma_2 & \lambda_2 & 0 \\ 0 & 0 & \lambda_3 \end{vmatrix} = 1 \Rightarrow \lambda_3 = (\lambda_1\lambda_2 - \gamma_1\gamma_2)^{-1} \tag{19}$$

With DIC measurements techniques, it is straightforward to determine the components of the deformation gradient, λ_k and γ_k . Substituting Eq. (19) into Eq. (2), gives

$$\begin{aligned} \sigma_{11} &= 2\left(\lambda_1^2 + \gamma_1^2 - \lambda_3^2\right)\Psi_{,1} - \left[\left(\lambda_2^2 + \gamma_2^2\right)\lambda_3^2 - \lambda_3^{-2}\right]\Psi_{,2} \\ \sigma_{12} &= 2\left(\lambda_1\gamma_2 + \lambda_2\gamma_1\right)\left(\Psi_{,1} + \lambda_3^2\Psi_{,2}\right) \\ \sigma_{22} &= 2\left(\lambda_2^2 + \gamma_2^2 - \lambda_3^2\right)\Psi_{,1} - \left[\left(\gamma_1^2 + \lambda_1^2\right)\lambda_3^2 - \lambda_3^{-2}\right]\Psi_{,2} \end{aligned} \tag{20}$$

Cauchy stresses σ_{11}, σ_{12} and σ_{22} are inferred from the Eq. (5) as follows:

$$\begin{pmatrix} \sigma_{11} & \sigma_{12} \\ \sigma_{12} & \sigma_{22} \end{pmatrix} = \begin{pmatrix} \cos\theta & -\sin\theta \\ \sin\theta & \cos\theta \end{pmatrix} \begin{pmatrix} \sigma_{rr} & \sigma_{r\theta} \\ \sigma_{r\theta} & \sigma_{\theta\theta} \end{pmatrix} \begin{pmatrix} \cos\theta & \sin\theta \\ -\sin\theta & \cos\theta \end{pmatrix} \tag{21}$$

Where σ_{rr}, $\sigma_{r\theta}$ and $\sigma_{\theta\theta}$ are computed previously for given values of ξ, θ, U and J_m.
To estimate the partial derivatives, i.e. $\Psi_{,1}$ and $\Psi_{,2}$, we solve the system of Eqs. (21). If $\mathbf{X}$ is the unknown column vector that representing the partial derivatives, i.e. $\Psi_{,k}$ and σ the corresponding computed components of the Cauchy stress tensor, then Eqs.

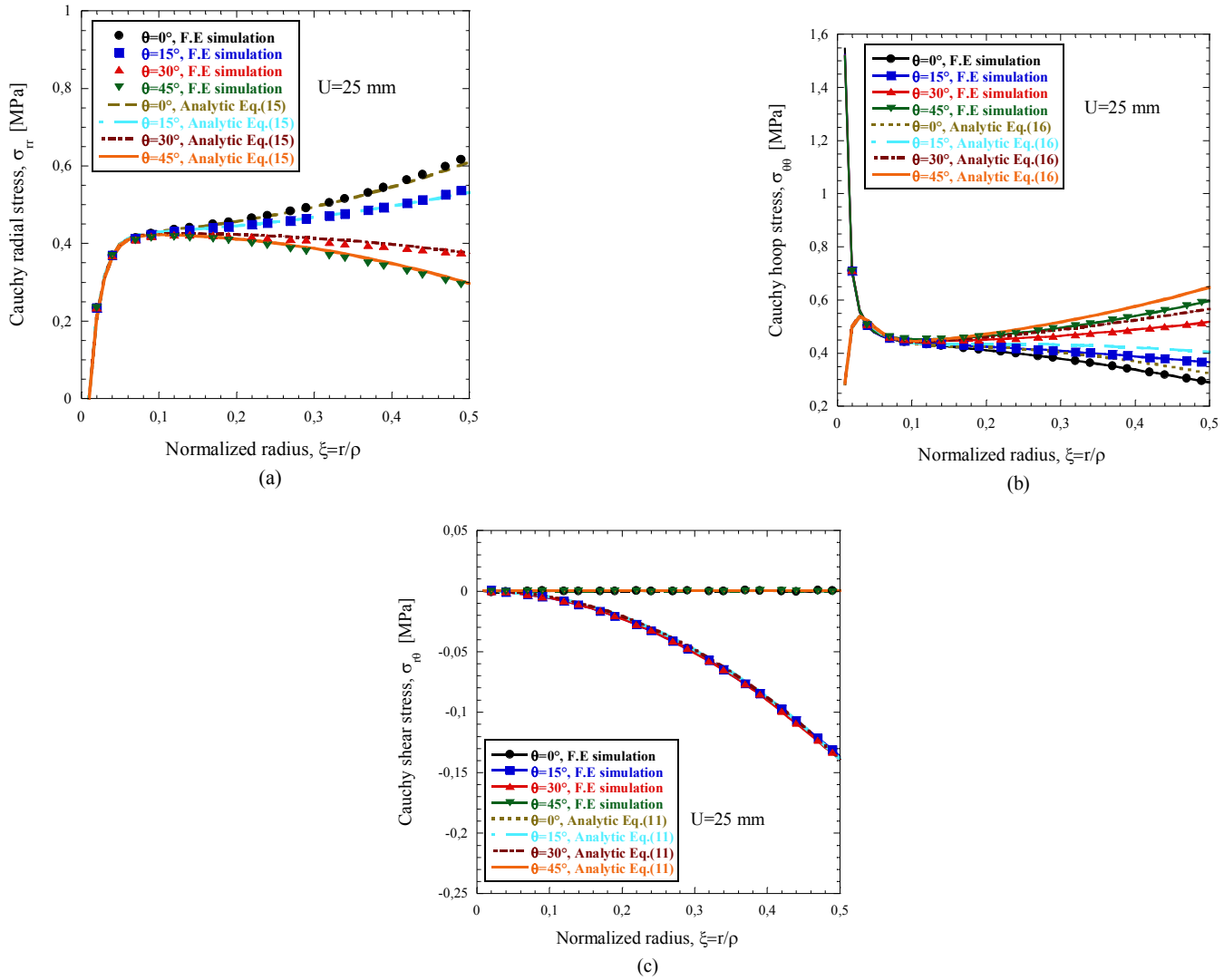

Fig. 7: (a) Comparison of the computed Cauchy radial stress $\sigma_{r\theta}(\xi, \theta)$ and simulated numerically by FE, versus normalized radius ξ and for different values of θ; (b) Comparison of the computed Cauchy hoop stress $\sigma_{rr}(\xi, \theta)$ and simulated numerically by FE, versus normalized radius ξ and for different values of θ; (c) Comparison of the computed Cauchy shear stress $\sigma_{\theta\theta}(\xi, \theta)$ and simulated numerically by FE, versus normalized radius ξ and for different values of θ

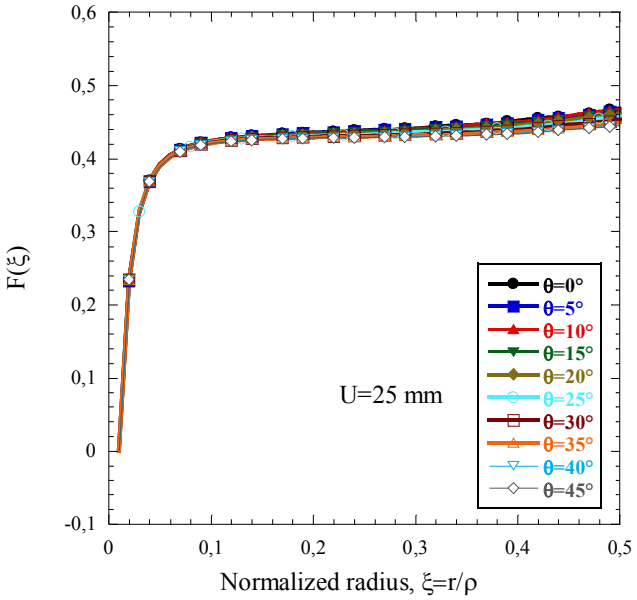

Fig. 8: Graphs of the function $F(\xi)$ versus ξ for different values of θ

(20) can be written as follows:

$$\mathbf{A}\,\mathbf{X} = \boldsymbol{\sigma} \tag{22}$$

where $\mathbf{A}$ is the 3×2 matrix of the linear system of Eqs. (20).
The right-hand side vector $\boldsymbol{\sigma}$ is contaminated by noise (error $\mathbf{e}$), which originates from computation of Cauchy stresses and measurement errors. The solution of Eq. (22) becomes ill-posed if the matrix $\mathbf{A}$ is not invertible; noting that $\mathbf{A}$, is not square. Mostly, the solution of an ill-posed problem without numerical stabilization is not acceptable **?**. A least squares fit of Eq. (22) is performed by first multiplying both sides with the transpose of $\mathbf{A}$:

$$\left(\mathbf{A}^T\mathbf{A}\right)^{-1}(\mathbf{A}^T\mathbf{A})\mathbf{X} = \left(\mathbf{A}^T\mathbf{A}\right)^{-1}\mathbf{A}^T\boldsymbol{\sigma} \tag{23}$$

Eq. (24) is the solution in the least squares sense, and the hyperelastic functions $\mathbf{X}$ are determined with minimizing the square of the sums of the squares of the differences between experimental and theoretical stresses at different strain values (error $\mathbf{e}^2 = e^T\mathbf{e}$) leading to the best fit:

$$\mathbf{X} = \left(\mathbf{A}^T\mathbf{A}\right)^{-1}\mathbf{A}^T\boldsymbol{\sigma} \tag{24}$$

4 Conclusion

An original method has been developed in order to compute the Cauchy stress field around a small hole located in the center of a cruciform specimen, which is subjected to equibiaxial tensile test (stretch ratio $1/1$). It has been shown that, both the stress and strain fields are heterogeneous in the core region; the heterogeneity seems to be an advantage for parameter identification. To improve the accurate parameter identification, an analytical relationship has been established between the applied forces on the sample edges and Cauchy local stresses. We emphasize that, the strain-energy density of a rubber-like material could be obtained directly from experimental data arising from this heteregeneous test. Also, the experimental data of this test could be used for the validation of a given constitutive model. We recall that the first and second principal invariants, i.e. I_1 and I_2 are identical in the range of small deformations. As a result, the partial derivatives are very sensitive to experimental noise; thereby, the parameter-identification becomes then ill-posed problem. Besides, the present analysis could be validated experimentally, that will an interesting challenge.

Acknowledgment

This research did not receive any specific grant from funding agencies in the public, commercial, or non-for-profit sectors.

Appendix A: Computation of the Cauchy stresses

The equilibrium equations are given by

$$\frac{\partial}{\partial\theta}\left(r\frac{\partial\sigma_{rr}}{\partial r}+\sigma_{rr}\right)=-\left(2\sigma_{r\theta}+r\frac{\partial\sigma_{r\theta}}{\partial r}+\frac{\partial^2\sigma_{r\theta}}{\partial\theta^2}\right) \tag{A.1}$$

$$\sigma_{\theta\theta}=\frac{\partial\sigma_{r\theta}}{\partial\theta}+r\frac{\partial\sigma_{rr}}{\partial r}+\sigma_{rr} \tag{A.2}$$

$$\sigma_{r\theta}=-\sigma_U h\left(\xi\right)\ \sin 4\theta,\ \text{for}\ \theta\neq 0,\ \pi/4\ \text{and}\ \pi/2 \tag{A.3}$$

By substituting Eq. (A.3) into Eq. (A.1), we obtain the following differential equation

$$\xi\frac{\partial\sigma_{rr}}{\partial\xi}+\sigma_{rr}=\frac{\sigma_U}{4}\left(14h\left(\xi\right)-\xi\,h'\left(\xi\right)\right)\cos 4\theta+f\left(\xi\right) \tag{A.4}$$

The solution of Eq. (A.4) is

$$\sigma_{rr}\left(\xi,\theta\right)=A\left(\xi,\theta\right)\xi^{-1}=\Omega\left(\xi,\theta\right)+\xi^{-1}N\left(\theta\right) \tag{A.5}$$

where

$$\Omega\left(\xi,\theta\right)=\left(\beta\frac{\sigma_U}{4}\lambda\right)\ \left(4\xi^2+14\xi_a^2-13\xi_a\xi\right)\cos 4\theta+F\left(\xi\right) \tag{A.6}$$

where $F\left(\xi\right)$ is a function to be determined and related to the function $f\left(\xi\right)$.
The boundary condition leads to $\sigma_{rr}\left(\xi_a,\theta\right)=0$

$$N\left(\theta\right)=\left(-\frac{5}{4}\beta\sigma_U\lambda\right)\xi_a^3\cos 4\theta \tag{A.7}$$

The radial Cauchy stress is given by

$$\sigma_{rr}\left(\xi,\theta\right)=\left(\beta\frac{\sigma_U}{4}\lambda\right)\ \left(4\xi^2+14\xi_a^2-13\xi_a\xi-5\xi_a^3\xi^{-1}\right)\cos 4\theta+F\left(\xi\right) \tag{A.8}$$

where $F\left(\xi\right)$is inferred from the results of FE-simulations of radial Cauchy stress.
The graphs of the function $F\left(\xi\right)=\sigma_{rr}\left(\xi,\theta\right)-\left(\beta\frac{\sigma_U}{4}\lambda\right)\ \left(4\xi^2+14\xi_a^2-13\xi_a\xi-5\xi_a^3\xi^{-1}\right)\cos 4\theta$ versus ξ for different values of θ are shown in Fig. 8.
This function can be approximated by

$$F\left(\xi\right)=\sigma_U\sqrt{\lambda}\,\Upsilon\left(\lambda\right),\ \Upsilon\left(\lambda\right)=a\left[1-e^{-b\left(\xi-\xi_a\right)}\right]+c\left(\xi-\xi_a\right) \tag{A.9}$$

where the constants $a=0.4,\ b=67$ and $c=0.06.$.
The hoop stress is inferred from Eq. (A.2) as follows:

$$\sigma_{\theta\theta}\left(\xi,\theta\right)=\left(\beta\frac{\sigma_U}{4}\lambda\right)\ \left(-4\xi^2-2\xi_a^2+6\xi_a\xi\right)\ \cos 4\theta+F\left(\xi\right)+\xi\ F'\left(\xi\right) \tag{A.10}$$

Tab. A.1: Model parameters values

parameter	value
c_{10} [MPa]	0.111
c_{01} [MPa]	0.039
μ_0 [MPa]	0.9
κ_0[MPa]	10000

References

L. Chevalier, S. Calloch, F. Hild, and Y. Marco. Digital image correlation used to analyze the multiaxial behavior of rubber-like materials. *European Journal of Mechanics-A/Solids*, 20(2):169–187, 2001.

C. Galliot and R.H. Luchsinger. Uniaxial and biaxial mechanical properties of etfe foils. *Polymer testing*, 30(4):356–365, 2011.

A.N. Gent. A new constitutive relation for rubber. *Rubber chemistry and technology*, 69(1):59–61, 1996.

Z. Guo and L.J. Sluys. Application of a new constitutive model for the description of rubber-like materials under monotonic loading. *International Journal of Solids and Structures*, 43(9):2799–2819, 2006.

S. Hartmann and R.R. Gilbert. Identifiability of material parameters in solid mechanics. *Archive of Applied Mechanics*, 88(1-2): 3–26, 2018.

S. Hartmann, R. R. Gilbert, and C. Sguazzo. Basic studies in biaxial tensile tests. *GAMM-Mitteilungen*, 41(1):e201800004, 2018.

F. Hild and S. Roux. Digital image correlation: from displacement measurement to identification of elastic properties–a review. *Strain*, 42(2):69–80, 2006.

G.A. Holzapfel. *Nonlinear Solid Mechanics: A Continuum Approach for Engineering*, 2000.

C.O. Horgan and G. Saccomandi. Pure axial shear of isotropic, incompressible nonlinearly elastic materials with limiting chain extensibility. *Journal of elasticity*, 57(3):307–319, 1999.

C.O Horgan and G. Saccomandi. Pure azimuthal shear of isotropic, incompressible hyperelastic materials with limiting chain extensibility. *International journal of non-linear mechanics*, 36(3):465–475, 2001.

J.-J. Hu, G.-W. Chen, Y.-C. Liu, and S.-S. Hsu. Influence of specimen geometry on the estimation of the planar biaxial mechanical properties of cruciform specimens. *Experimental Mechanics*, 54(4):615–631, 2014.

M. Johlitz and S. Diebels. Characterisation of a polymer using biaxial tension tests. Part I: Hyperelasticity. *Archive of Applied Mechanics*, 81(10):1333–1349, 2011.

M. Mooney. A theory of large elastic deformation. *Journal of applied physics*, 11(9):582–592, 1940.

R.W. Ogden. *Non-Linear Elastic Deformations*. Courier Corporation, New York, 1997.

N. Promma, B. Raka, M. Grediac, E. Toussaint, J.-B. Le Cam, X. Balandraud, and F. Hild. Application of the virtual fields method to mechanical characterization of elastomeric materials. *International Journal of Solids and Structures*, 46(3-4):698–715, 2009.

M. Sasso, G. Palmieri, G. Chiappini, and D. Amodio. Characterization of hyperelastic rubber-like materials by biaxial and uniaxial stretching tests based on optical methods. *Polymer Testing*, 27(8):995–1004, 2008.

H Seibert, T Scheffer, and S Diebels. Biaxial testing of elastomers-experimental setup, measurement and experimental optimisation of specimen's shape. *Technische Mechanik*, 34(2):72–89, 2014.

J.C. Simo and T.JR. Hughes. *Computational inelasticity*, volume 7. Springer Science & Business Media, 2006.

S. Timoshenko. *Theory of Elasticity*. McGraw Hill Book Co., New York Toronto London, 1951.

W. Zhang, Y. Feng, C.-H. Lee, K. L. Billiar, and M. S. Sacks. A generalized method for the analysis of planar biaxial mechanical data using tethered testing configurations. *Journal of biomechanical engineering*, 137(6):064501, 2015.